Nanoscale

ROYAL SOCIETY OF CHEMISTRY

COMMUNICATION

View Article Online
View Journal | View Issue

Cite this: *Nanoscale*, 2024, **16**, 14730

Received 30th March 2024,
Accepted 11th July 2024

DOI: 10.1039/d4nr01402b

rsc.li/nanoscale

Substrate-induced phase transition within liquid condensates reverses the catalytic activity of nanoparticles†

S. M. Rose, [a] Silky Bedi, [a] Sabyasachi Rakshit *[b] and Sharmistha Sinha *[a]

Liquid–liquid phase separation is reported to enhance the catalytic reaction rates severalfold. Herein, we explored the interactions between a catalyst and a range of substrate concentrations to understand the impact on the droplet phase and catalytic reaction kinetics. We observed that the substrate above a critical concentration induces phase transitions within liquid condensates and restricts the free movement of both the substrate and products, resulting in an overall reduction of the reaction rate, an observation not reported earlier.

Introduction

Dynamic assemblies of biopolymers (protein/nucleic acid) orchestrated through liquid–liquid phase separation (LLPS) are referred to as biomolecular condensates. Investigations conducted in recent years reveal that these condensates serve as organisers for various biochemical processes, including cell signalling, transcription, stress response and enzyme catalysis. Condensates engaged in enzyme catalysis are further subclassed as catalytic condensates, which sequestrate catalysts inside a small volume, leading to a significantly elevated local concentration of the catalyst.[1,2] Consequently, the turnover of the reaction is enhanced severalfold. For example, glycolytic enzymes in cells form catalytic condensates (glycolytic bodies/G bodies) under hypoxic conditions to increase the rate of glycolysis. Similarly, six enzymes involved in *de novo* purine biosynthesis assemble in purinosomes and increase the production of nucleotides.[3,4]

In recent years, extensive research has been dedicated to mimicking catalytic condensates *in vitro* and have consistently demonstrated improved rate kinetics.[5–8] This enhanced rate is attributed to the increased proximity or local concentration of reacting molecules in the condensate. Furthermore, the reported enhancement in catalytic reactions is based on the single-point concentration of the substrate and catalyst.[1,5] Importantly, the concentration of small molecules (substrates) can significantly alter the driving forces of LLPS (transient and non-covalent interactions).[9–11] Consequently, the phase of the condensate changes, potentially affecting its viscoelastic properties and the dynamics of substrate channelling during the reaction.[2,12] However, the present body of literature lacks comprehensive studies elucidating the impact of substrate concentration on the kinetics of these catalytic condensates. Herein, we systematically vary the substrate concentration and derive the effect on catalytic reaction kinetics in liquid condensates. We obtained a non-linear change in the kinetics and correlated it with the phase behaviour of liquid condensates. We opted for a low-cost, readily synthesizable BSA-gold nanocluster (AuNC@BSA) as a catalyst and the oxidation of pyrogallol as a model reaction.[13,14] Furthermore, the catalyst exhibits the ability to undergo LLPS and has demonstrated an enhanced reaction-rate in condensates for a particular substrate concentration.[15] Overall, our findings here pave the way to understand the effect of small biological molecules (*e.g.*, nucleotides, amino acids or other metabolites) on the reaction kinetics in the condensate phase.

Results and discussion

As reported, we synthesized AuNC@BSA through the reduction of Au^{3+} ions using BSA as a reducing and stabilising agent.[16,17] The formation of AuNC@BSA was confirmed by an emission peak at 670 nm when excited at 450 nm (Fig. 1a) as well as by agarose gel electrophoresis (inset, Fig. 1a). We induced the LLPS of AuNC@BSA using 5% (w/v) PEG6000 in 500 mM of kosmotropic salt, Na_2SO_4. To follow the formation of liquid droplets, we labelled 1% of BSA with Texas Red (TR) and monitored fusion events under a fluorescence microscope (Fig. 1b).

[a]*Chemical Biology Unit, Institute of Nano Science and Technology, Sector 81, SAS Nagar, Punjab-140306, India. E-mail: sinhas@inst.ac.in*
[b]*Department of Chemical Sciences, Indian Institute of Science Education and Research, Sector 81, SAS Nagar, Punjab-140306, India. E-mail: srakshit@iisermohali.ac.in*

†Electronic supplementary information (ESI) available. See DOI: https://doi.org/10.1039/d4nr01402b

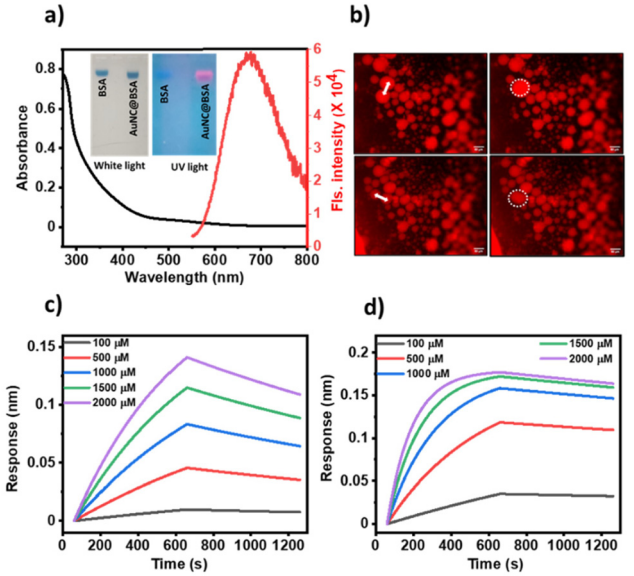

Fig. 1 Characterisation and phase separation of AuNC@BSA: (a) UV-vis and fluorescence spectra of AuNC@BSA. Inset shows agarose gel electrophoresis of BSA and AuNC@BSA loaded with Coomassie blue under white and UV light. Colocalization of blue (from Coomassie blue) and red (from AuNCs) suggest the presence of AuNCs with BSA, (b) fluorescence images of TR-labelled AuNC@BSA condensates featuring fusion events (white double-headed arrow indicates fusing droplets). BLI studies of (c) BSA, (d) AuNC@BSA at different concentrations of pyrogallol showing high affinity of pyrogallol towards AuNC@BSA with a K_D value of (35.1 ± 3.2) × 10^{-6} M in comparison to BSA with K_D = (66.7 ± 2.0) × 10^{-5} M.

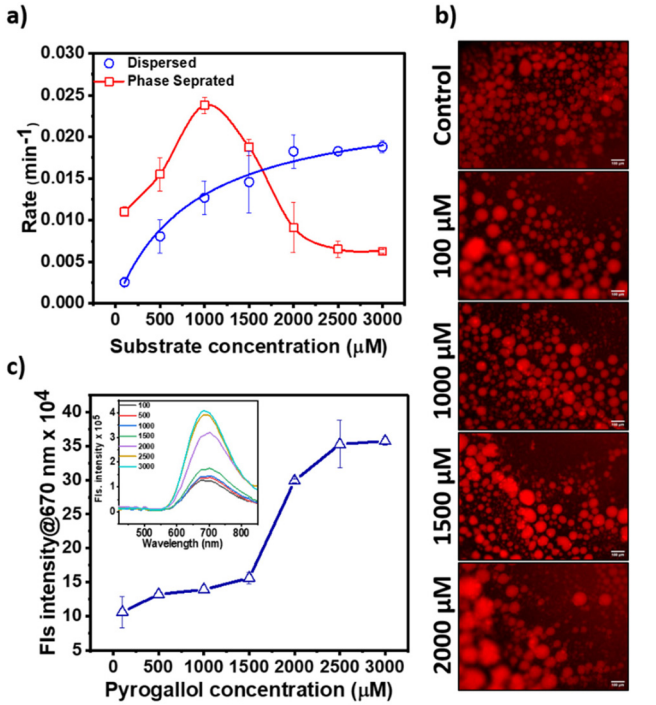

Fig. 2 (a) Kinetics of the oxidation of pyrogallol to purpurogallin catalysed by the BSA-Gold nanocluster (AuNC@BSA) in the presence of high excess H_2O_2 (0.1 M) in dispersed and phase separated (PS) conditions, (b) fluorescence microscopy images of Texas red labelled AuNC@BSA in the absence (control) and presence of different concentrations (100 μM, 1000 μM, 1500 μM and 2000 μM) of pyrogallol. Images are taken after starting the oxidation reaction by the addition of H_2O_2. Scale bar is 100 μm. (c) Change in fluorescence of AuNC@BSA with increasing concentration of pyrogallol.

Furthermore, using biolayer interferometry,[18] we probed the interaction of the substrate with the catalyst. 1 mg ml^{-1} of AuNC@BSA or BSA was loaded on the activated amine reactive second generation (AR2G) sensor and the association and dissociation kinetics were recorded by immersing the receptor-loaded sensor in different concentrations of pyrogallol and water. We obtained dissociation constants (K_D) of (35.1 ± 3.2) × 10^{-6} M for the interaction of pyrogallol-AuNC@BSA, and (66.7 ± 2.0) × 10^{-5} M for pyrogallol-BSA (Fig. 1c and d). The micromolar range of the dissociation constant indicates reversible binding between the substrate and the catalyst. These interaction studies also indicate that in addition to the catalytic sites on the AuNCs, the protein BSA can also harbour the substrate through at orders of magnitude weaker affinity.

AuNC@BSA catalysts exhibited Michaelis–Menten kinetics in the dispersed phase consistent with previous reports. However, under phase-separated conditions, the reaction rates followed a bell-shaped curve with increasing substrate concentration (Fig. 2a). We observed a notable 2 to 5-fold increase in the reaction rate within the 100 μM to 1000 μM substrate concentration range, followed by a gradual decline and saturation at 2000 μM to 3000 μM, respectively (Table S1† and Fig. 2a). While the initial increase in the catalytic rate can be attributed to the enhanced local concentrations of both, the substrate and catalyst within the condensates, the subsequent decrease in the reaction rate remains unclear. To decipher the underlying reason for the drop in the reaction rate, we first estimated the partitioning of the substrate between the dispersed phase and condensed phase. The partition coefficient remains unaltered with increasing substrate concentrations, indicating no bias in the substrate uptake by the condensates (Fig. S1†). Furthermore, we did not observe any change in the droplet integrity and size with increasing substrate concentration (Fig. 2b and Table S2†).

Next, we probed the effect of the substrate on catalysts and monitored the fluorescence intensity of the AuNC@BSA at 670 nm with increasing amounts of pyrogallol. We observed a typical sigmoidal feature, a gradual increase in the fluorescence intensity with increasing pyrogallol concentration (100–1500 μM), followed by a sudden jump above 1500 μM. The intensity reaches a saturation above 2500 μM (Fig. 2c). It is known that Au-nanoclusters exhibit higher emission in non-polar solvents compared to that in polar.[19] We argue that pyrogallol binds with BSA and screens solvent accessibility for AuNC@BSA, thus gradually enhancing the hydrophobicity within the droplet and around AuNC@BSA. We already measured a weak interaction of pyrogallol with BSA using BLI. To understand the nature of interactions, we docked BSA (PDB

ID 3V03) and pyrogallol using AutoDock Vina, and identified several possible sites of interactions that may support our argument (Fig. S2†). The observed docking complexes indicate that the hydroxyl groups of pyrogallol are engaged in hydrogen bonding interactions with several residues in BSA (bovine serum albumin). This interaction suggests that the hydroxyl groups are shielded by these interactions, potentially leading to an enhancement in hydrophobicity. This shielding effect could arise from the formation of hydrogen bonds between the hydroxyl groups of pyrogallol and specific amino acid residues in BSA, which might alter the overall hydrophobic character of the system.

Furthermore, it is reported that the fluorescence intensity of AuNC@BSA increases with the phase separation to a higher-order aggregation.[22] We too observed a step-wise increase in fluorescence intensity beyond 1500 μM of the substrate concentration, followed by saturation, indicative of the phase transition. The catalytic rate also declines within this concentration range. Based on these findings, we propose that the hydrophobic environment within the droplets facilitates a phase transition from a liquid state to a crystalline phase. This crystalline phase could impede the efficient channelling of the substrate and product, resulting in a decrease in reaction kinetics (see Fig. 2a). To test our hypothesis, we first measured the rate of droplet formation of AuNC@BSA with and without pyrogallol from the turbidity assay (scattering at 700 nm). We found that the condensate forming rate is twice in the presence of 2000 μM pyrogallol (Fig. 3a). The faster rate indicates

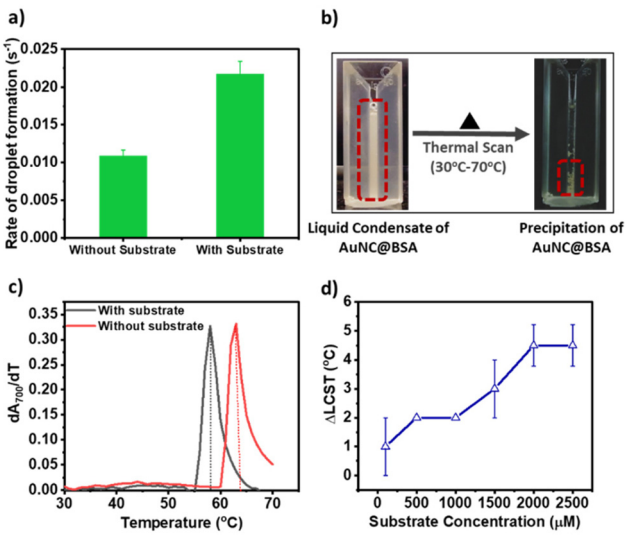

Fig. 3 Effect of the substrate on the phase behaviour of AuNC@BSA: (a) rate of formation of the droplet monitored by measuring the change in turbidity with respect to time at 700 nm, (b) condensates of AuNC@BSA undergoes liquid to the solid phase transition on increasing temperature. The phase transition was monitored by measuring turbidity at 700 nm using a UV-vis spectrophotometer and the transition is LCST (lower critical solution temperature) type. (c) LCST of the liquid to the solid phase transition of AuNC@BSA in the absence and presence of the substrate (2000 μM). (d) The difference of LCST (ΔLCST) in the absence and presence of various concentrations of the substrate.

that the presence of the substrate molecule facilitates faster ageing of the condensates. Faster ageing may lead to the faster phase separation of the liquid condensates to a solid-like phase, a phenomenon commonly noticed in amyloids. Secondly, we measured the lower critical solution temperature (LCST) of the liquid condensates. For this, we gradually heated the phase-separated mixture and monitored the temperature above which the liquid condensates of AuNC@BSA separated into two immiscible phases as seen in Fig. 3b.

At lower temperatures, robust solvent–solute interactions, primarily through hydrogen bonding, yield a negative enthalpy of mixing. Consequently, this results in an overall negative change in the free energy mixing, thus maintaining solubility at lower temperatures. However, upon heating beyond the LCST, these solvent–solute interactions are disrupted. Instead, entropically driven interactions, such as hydrophobic interactions between solute molecules, become dominant. This transition leads to phase separation, transforming the initially miscible liquid into an immiscible solid phase.[20,21] Here, we estimated the LCST for AuNC@BSA condensates at each pyrogallol concentration by measuring turbidity at 700 nm while heating the mixture. LCST was calculated from the differential change in turbidity with temperature (as shown in (dA_{700}/dT) *vs.* temperature plot in Fig. 3c). In the absence of any substrate, the LCST of the droplets was 62 ± 1 °C and decreased gradually upon increasing the substrate concentration (Fig. 3c). We measured the difference of LCST between the no-substrate to the substrate ($\Delta LCST = LCST_{no\ substrate} - LCST_{substrate}$) and plotted the change in ΔLCST with increasing substrate concentration. We observed a gradual increase in the ΔLCST value up to 1000 μM, followed by a sudden jump thereafter until 2000 μM and saturation (Fig. 3d). The trend ΔLCST corresponds to the change in fluorescent intensity of AuNC@BSA with the increasing substrate, and supports our hypothesis of phase behaviour alteration within the condensates.

Our observations suggest that once the substrate concentration surpasses a critical threshold, the internal environment within the liquid condensates undergoes changes, influencing the dynamics of the solvent. This alteration impedes the free movement of both substrate and products, resulting in an overall reduction in the reaction rate.

Conclusions

This study investigated the intricate interaction dynamics between pyrogallol and AuNC@BSA catalysts across varying substrate concentrations. At lower concentrations, weaker interactions limit significant phase transitions, while reaction rates remain higher within the condensed phase. As the substrate concentration increases, stronger interactions initiate the phase transitions impacting both reaction kinetics and ΔLCST values. The sigmoidal increase in the fluorescence intensity observed from 1500 μM signifies a less sensitive response to initial phase transitions compared to ΔLCST and

reaction rate measurements. Complete phase transition at higher substrate saturates fluorescence intensity and ΔLCST, correlating with decreased reaction rates due to altered dynamics in the condensed phase.

Our studies have revealed that catalytic reactions occurring within liquid condensates do not adhere to the classical Michaelis–Menten kinetics model. This departure from the traditional enzymatic kinetics underscores the unique nature of biochemical processes within the condensed phases, where factors such as spatial confinement and altered microenvironments play significant roles in modulating reaction kinetics. These findings emphasize the critical importance of considering the substrate concentration when studying the reaction rates within catalytic condensates. Moreover, phase-separated catalytic condensates demonstrate significant potential for applications in energy,[23] environment,[24] biotechnology sectors,[8] and enhancing reaction kinetics. However, for effective *in vitro* catalysis, modifying catalytic surfaces or supplementing systems with small molecules is crucial to restrict further phase transitions in condensates without compromising reaction rates. In sum, these findings not only advance a fundamental understanding of reaction dynamics within condensates but also offer practical insights into manipulating and emulating biological systems.

Author contributions

SM Rose: experimental design and execution, methodology, data analysis, investigation, original manuscript drafting and editing. Silky Bedi: experiment execution, manuscript editing. Sabyasachi Rakshit: conceptualization and manuscript writing. Sharmistha Sinha: supervision, conceptualization, writing – reviewing and editing.

Data-availability

Part of the data supporting the findings of the manuscript is presented in the ESI.† Additional data if required will be available on request.

Conflicts of interest

There are no conflicts to declare.

Acknowledgements

SMR acknowledges INST for financial support and all the research facilities. SB acknowldeges DST-INSPIRE for fellowship.

References

1 B. Saini and T. K. Mukherjee, *J. Phys. Chem. B*, 2023, **127**, 180–193.
2 B. G. O'Flynn and T. Mittag, *Curr. Opin. Cell Biol.*, 2021, **69**, 70–79.
3 H. Zhao, C. R. Chiaro, L. Zhang, P. B. Smith, C. Y. Chan, A. M. Pedley, R. J. Pugh, J. B. French, A. D. Patterson and S. J. Benkovic, *J. Biol. Chem.*, 2015, **290**, 6705–6713.
4 A. M. Pedley, J. P. Boylan, C. Y. Chan, E. L. Kennedy, M. Kyoung and S. J. Benkovic, *J. Biol. Chem.*, 2022, **298**, 101845.
5 A. M. Küffner, M. Prodan, R. Zuccarini, U. Capasso Palmiero, L. Faltova and P. Arosio, *ChemSystemsChem*, 2020, **2**, e2000001.
6 M. Guan, M. V. Garabedian, M. Leutenegger, B. S. Schuster, M. C. Good and D. A. Hammer, *Biochemistry*, 2021, **60**, 3137–3151.
7 M. Liu, S. He, L. Cheng, J. Qu and J. Xia, *Biomacromolecules*, 2020, **21**, 2391–2399.
8 S. Lim and D. S. Clark, *Trends Biotechnol.*, 2023, **42**, 496–509.
9 S. Li, Y. Wang and L. Lai, *Acta Biochim. Biophys. Sin.*, 2023, **55**, 1075–1083.
10 W. M. Babinchak, B. K. Dumm, S. Venus, S. Boyko, A. A. Putnam, E. Jankowsky and W. K. Surewicz, *Nat. Commun.*, 2020, **11**, 5574.
11 K. L. Saar, A. S. Morgunov, R. Qi, W. E. Arter, G. Krainer, A. A. Lee and T. P. J. Knowles, *Proc. Natl. Acad. Sci. U. S. A.*, 2021, **118**, e2019053118.
12 S. F. Banani, H. O. Lee, A. A. Hyman and M. K. Rosen, *Nat. Rev. Mol. Cell Biol.*, 2017, **18**, 285–298.
13 Y. Song, J. Qiao, W. Liu and L. Qi, *Microchem. J.*, 2020, **157**, 104871.
14 R. Ahmad, J. Shanahan, S. Rizaldo, D. S. Kissel and K. L. Stone, *Catalysts*, 2020, **10**, 499.
15 S. Bedi, G. Kumar, S. M. Rose, S. Rakshit and S. Sinha, *Chem. Commun.*, 2022, **58**, 8634–8637.
16 S. Govindaraju, S. R. Ankireddy, B. Viswanath, J. Kim and K. Yun, *Sci. Rep.*, 2017, **7**, 40298.
17 J. Xie, Y. Zheng and J. Y. Ying, *J. Am. Chem. Soc.*, 2009, **131**, 888–889.
18 R. L. Petersen, *Biosensors*, 2017, **7**, 49.
19 Z. Gan, J. Chen, J. Wang, C. Wang, M.-B. Li, C. Yao, S. Zhuang, A. Xu, L. Li and Z. Wu, *Nat. Commun.*, 2017, **8**, 14739.
20 Q. Sun, *Molecules*, 2022, **27**, 7009.
21 P. Paricaud, A. Galindo and G. Jackson, *Mol. Phys.*, 2003, **101**, 2575–2600.
22 A. Maity and A. Kumar, *Nanoscale Adv.*, 2022, **4**, 2988–2991.
23 Q. Liang, Y. Huang, Y. Guo, X. Zhang, X. Hu, H. Zeng, K. Liang, D. Zhao, L. Jiang and B. Kong, *Nat. Sustain.*, 2024, **7**, 628–639.
24 M. Yan, D. Ma, B. Qiu, T. Liu, L. Xie, J. Zeng, K. Liang, H. Xin, Z. Lian, L. Jiang and B. Kong, *Chem. – Eur. J.*, 2022, **28**, e202200307.